Time-Periodic Inertial Range Dynamics

Lennaert van Veen[*]
Faculty of Science, University of Ontario Institute of Technology, 2000 Simcoe Street North, Oshawa, L1H 7K4 Ontario, Canada

Alberto Vela-Martín[†]
School of Aeronautics, Universidad Politécnica de Madrid, 28040 Madrid, Spain

Genta Kawahara[‡]
Graduate School of Engineering Science, Osaka University, 1-3 Machikaneyama, Toyonaka, Osaka 560-8531, Japan

(Received 23 September 2018; published 27 September 2019)

A wide class of physical systems exhibit scale invariance. While the statistical properties of such behavior can often be investigated by theoretical and experimental means, its dynamics are notoriously hard to parse. We investigate scale-invariant dynamics through an unstable periodic orbit. This orbit coexists with turbulence of an incompressible fluid and yields a significant Kolmogorov energy spectrum. We identify events of intense energy transfer across spatial scales and relate them to vortical dynamics. The results support a recently proposed mechanism for turbulent energy transfer.

DOI: 10.1103/PhysRevLett.123.134502

Introduction.—The distribution of energy over spatial scales is central to the study of spatially extended physical systems. Power-law distributions are indicative of scale-invariant dynamics and are observed in a variety of phenomena, ranging from magnetic fluctuations in the solar wind [1] to mechanical vibrations of thunder sheets [2] and tangled vortex lines in superfluids [3]. In these systems, there exists a range of spatial scales in which the dynamics neither depend on the mechanism of energy input nor on the way it is dissipated. Ensemble averages of observables can often be predicted on the basis of dimensional analysis and compared to experimental data—indeed each of the papers cited above contain power-law distributions distilled from measurements. In contrast, the dynamical processes that conspire to produce this average behavior are ill understood. In this Letter, we study a minimal model for power-law behavior in a spatially extended system, namely large eddy simulation (LES) of homogeneous, isotropic turbulence (HIT), and show that its dynamics can be studied using a simple invariant solution as a proxy. To the best of our knowledge, this is the first investigation of scale-invariant dynamics using a simple invariant solution, and it presents a promising step forward for the study of systems with a wide range of active spatial scales.

Arguably the most famous example of a power-law energy spectrum is Kolmogorov's "law of $-5/3$" for HIT [4]. It was derived for the *inertial range* of spatial scales, which are smaller than the scales that characterize interaction with material boundaries or a body force, but larger than that on which viscous damping is dominant, under the assumption that the statistical properties of the flow are determined entirely by the rate of energy dissipation. Although corrections to the exponent of $-5/3$ arise due to intermittent energy dissipation events [5], it was shown to fit experimental and numerical data well [6–8]. The statistics of inertial range turbulence are thus well studied, but the nature of turbulent dynamics remains one of the great open questions of physics.

The beginning of an answer is that turbulence is not featureless but populated by structures, like vortex tubes and sheets, which stay coherent over long enough times to consider them "building blocks." Such structures are distributed across scales and their interaction is thought to be essential to the processes of the energy cascade. One picture consistent with a power-law spectrum, often attributed to Richardson [9], is that these structures "break down" in a self-similar fashion, thereby transferring energy to progressively smaller scales. Various mechanisms have been proposed for such break-down, for instance the ejection of thin, spiral vortex filaments from a large-scale vortex tube [10], the generation of counter-rotating vortex pairs wrapped around such a structure [11] and, more recently, the iterated flattening and roll-up of vortex filaments [12]. What these mechanisms have in common, is that the transport of a given amount of energy across the inertial range takes a finite time. This time delay explains the quasicyclic behavior of spatial mean quantities, like the total energy and its rate of dissipation, observed both in experiments and in simulations (e.g., [13–15]). In the first

phase of the cycle, large-scale space structures grow under the influence of the forcing. In the next phase, these structures break down, thus supporting the energy cascade. Finally, the large scales of the flow enter a quiescent state. This process repeats with a period much greater than the large-eddy turnover time. In various contexts the question has been posed whether this regeneration cycle of turbulence could be represented by a time-periodic solution to the governing equations [12,16,17]. We answer this question to the affirmative by presenting an unstable periodic orbit (UPO) that exhibits the expected regenerative dynamics as well as the statistics of developed turbulence.

LES of box turbulence.—The width of the inertial range in HIT is expected to grow as $\mathrm{Re}_\lambda^{3/4}$, where Re_λ is Taylor's microscale Reynolds number. At the minimal value of Re_λ for which a significant Kolmogorov spectrum is observed, around $\mathrm{Re}_\lambda = 100$, a faithful direct numerical simulation (DNS) requires several millions of degrees of freedom (DOF), which exceeds the limits of our current numerical methods for computing UPOs. We mitigate this problem by modeling the effect of the small-scale motion by an effective eddy viscosity. The resulting equations are

$$\partial_t \boldsymbol{u} + \boldsymbol{u}\cdot\nabla\boldsymbol{u} + \nabla\left(\frac{p}{\rho} + \frac{1}{3}\Pi\right) - 2\nabla(\nu_T \boldsymbol{S}) = \gamma \boldsymbol{f}, \quad (1)$$

$$\nabla\cdot\boldsymbol{u} = 0, \quad (2)$$

where $\boldsymbol{u}$, p, and $\boldsymbol{S}$ are the grid-scale velocity, pressure, and rate-of-strain tensor, respectively, and Π contains the normal subgrid stress. The density, ρ, the forcing, $\boldsymbol{f}$, and its amplitude, γ, are constant. Using the closure proposed by Smagorinsky [18], the eddy viscosity is given by

$$\nu_T = (C_\mathrm{S}\Delta)^2\sqrt{2S_{ij}S_{ij}}, \quad (3)$$

where C_S is the Smagorinsky parameter, Δ is the grid spacing, and summation over repeated indices is implied. While energy is removed from the system in an artificial way, this closure has been shown to faithfully reproduce inertial range dynamics and statistics, including spatial intermittency, in the presence of periodic boundary conditions [19–21]. The force is $\boldsymbol{f} = (-\sin(x)\cos(y), \cos(x)\sin(y), 0)^T$, as used by Yasuda *et al.* [16], on a $2\pi \times 2\pi \times 2\pi$ periodic cube. The governing equations inherit the symmetries of this force so they are equivariant under translations in the z direction. Results below are scaled with the integral length scale, $L = 3\pi\langle\int_0^\infty k^{-1}E(k,t)dk/(4K)\rangle_t$, the root-mean-squared velocity, given by $U^2 = 2\langle K\rangle_t/3$, and the large-eddy turnover time, $T = L/U$. Here, $K = \langle \boldsymbol{u}^2\rangle_s/2$, $E(k,t)$ is energy spectrum and $\langle . \rangle_{s,t}$ stands for the average in space (s), time (t), or both (st). These scales are commonly used in the study of HIT and we adopt them here for compatibility, even though the forcing is anisotropic. The local rate of energy transfer to the subgrid scales is denoted by $\epsilon = 2\nu_T S_{ij}S_{ij}$. Simulations are done with a pseudospectral code on 64^3 grid points, yielding a dynamical system with 230 243 DOF.

Embedded time-periodic motion.—The only parameter in this LES is C_S. When $C_\mathrm{S} \approx 1$, the fluid motion is temporally chaotic but has little spatial complexity because of the strong damping [22]. As we decrease C_S, the energy input and LES filter length scales become increasingly separated, allowing turbulence to develop. In more turbulent flow, the computation of time-periodic motion is more difficult. We employed the Newton-Krylov-hook algorithm [23] and its convergence hinges on a large portion of the DOF being strongly damped. Thus, the conditioning of the method deteriorates as C_S decreases. We selected an approximately time-periodic segment of simulation data in the strongly damped regime and gradually decreased C_S. At $C_\mathrm{S} = 0.55$, for a ratio of the integral length scale to the LES filter length of $L/(C_\mathrm{S}\Delta) \approx 24$, it took a few thousand Newton-hook iterations, each requiring a few hundred Krylov iterations, to obtain a periodic orbit that reproduces turbulent statistics and dynamics. The final residual is 3.5×10^{-5}, as measured by the energy of the difference between the final and the shifted initial state, normalized by the amplitude of the fluctuation of the energy along the UPO. The period of this UPO is about $9T$ and the shift in the vertical is 0.85Δ in one period. It has 210 ± 2 unstable Floquet multipliers, the uncertainty arising from the finite residual of the UPO. The largest multiplier in magnitude corresponds to a decorrelation time of $1.6T$. A projection of the UPO onto K and $\langle\epsilon\rangle_s$ is shown in Fig. 1. The white dots, drawn at regular time intervals, show that the state of the UPO is close to the centroid of the PDF of turbulence for about one third of its period. The average energy dissipation rate along the UPO is $\langle\epsilon\rangle_{st} = 0.508U^3/L$, within

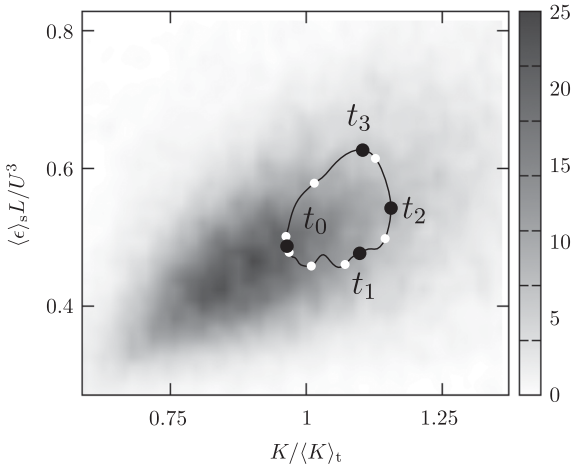

FIG. 1. Projection of the UPO onto K and $\langle\epsilon\rangle_s$, normalized by large scales. In gray scale the probability density function (PDF) of turbulent LES is shown. The structure of the flow at instants labeled t_0 and t_3 are shown in Fig. 3. The white dots have been drawn at regular time intervals $9T/7$.

0.5% from the average in LES turbulence and in good agreement with the range of values reported in the literature [24,25].

The time-averaged spectrum of the UPO, shown in Fig. 2, has a significant inertial range and agrees well with that of LES turbulence. Also shown is the spectrum of a DNS with the same forcing beyond the mixing transition, for which $\mathrm{Re}_\lambda = 111$ and $\langle\epsilon\rangle_{st} = 0.39U^3/L$, showing good agreement in the inertial range. We have included in Fig. 2 the anisotropy quantifier $Q(k) = A_{ij}A_{ij}/2$, where $A_{ij} = \langle E_{ij}(k,t)\rangle_t/\langle E(k,t)\rangle_t - \delta_{ij}/3$ is the spectral anisotropy tensor and $E_{ij}(k,t)$ is the cospectrum [26]. Anisotropy is high in the first wave number, but decreases for higher wave numbers to values typical of DNS with stochastic, approximately isotropic forcing, $Q \lesssim 0.01$ [26], and below values typical of experimental realizations, $Q \lesssim 0.15$ (e.g., [27]). The flow is fully 3D in the inertial scales and complies well with the local isotropy hypothesis of the Kolmogorov theory.

The structure of the time-periodic energy cascade.—We confirm the presence of an energy cascade in the UPO by analyzing the dynamics of the flow at different scales. We filter the velocity field and calculate energy fluxes in physical space, $s(\boldsymbol{x},t;l) = \tau_{ij}\bar{S}_{ij}$, where $\boldsymbol{x}$ is the spatial coordinate of the flow, $\bar{\cdot}$ denotes filtering at scale l with a Gaussian filter in Fourier space, $G(k) = \exp(-k^2l^2/24)$ [21], and $\tau_{ij} = \bar{u}_i\bar{u}_j - \overline{u_iu_j}$ is the subfilter stress tensor.

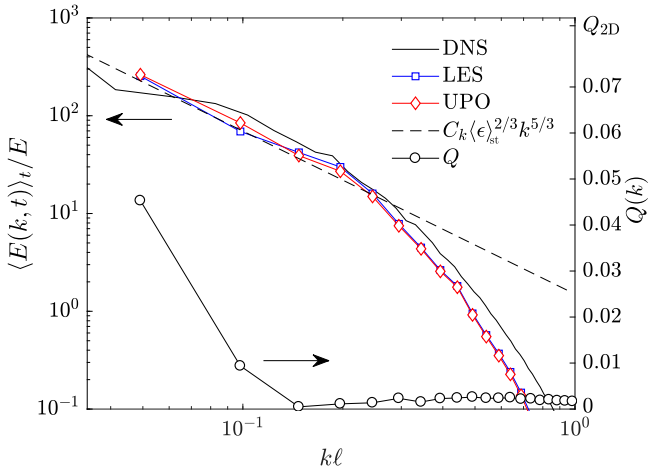

FIG. 2. Energy spectrum of the UPO and the anisotropy indicator Q. For comparison the spectra of turbulent LES and DNS, the latter with $\mathrm{Re}_\lambda = 111$, have been included, as well as the theoretically expected Kolmogorov spectrum with $C_k = 1.5$ (values in the range 1.3–1.7 have been reported [8]). The small-scale nondimensionalization is given by $E = [\langle\epsilon\rangle_{st}\langle\nu_T\rangle_{st}^5]^{1/4}$ and $\ell = [\langle\nu_T\rangle_{st}^3/\langle\epsilon\rangle_{st}]^{1/4}$ for LES and $E = [D\nu^5]^{1/4}$ and $\ell = [\nu^3/D]^{1/4}$ for DNS, where $D = 2\nu\langle S_{ij}S_{ij}\rangle_{st}$ is the energy dissipation rate and ν is the kinematic viscosity. $Q_{2D} = 1/12$ is the anisotropy of a 2D Taylor-Green vortex of the form $\boldsymbol{f}$. The left (right) arrow refers to the logarithmic (linear) scale on the vertical axis.

Negative $s(\boldsymbol{x},t)$ indicates that energy is flowing towards the small scales. In addition, we consider the enstrophy, $\boldsymbol{\omega}^2$, and the enstrophy of the filtered field, $\bar{\boldsymbol{\omega}}^2$, where $\boldsymbol{\omega} = \nabla\times\boldsymbol{u}$ is the vorticity vector.

Visual inspection of these quantities reveals at least two generations of vortices at the integral scale and the subgrid filter scale, shown at $t = t_0$ and t_3 in Fig. 3. The first takes the form of four large counter-rotating vortex columns. Although generated and constrained by the forcing, these column vortices change considerably in intensity, wind and meander, interact with the next generation of vortices, and display complex, three-dimensional dynamics in time. The next generation of vortices, visualized with the isosurfaces of unfiltered enstrophy, populate the vicinity of the first and appear mostly perpendicular to these. We hypothesize that the smaller vortices are stretched in the vicinity of columnar vortices by the strong magnitude of the rate-of-strain tensor generated by the latter [28]. Intense energy transfer at the scale of the large vortices, $l = 1.6L$, is also located in this region, suggesting a connection of this mechanism with the energy cascade. We observe that the vortices at the grid scale reproduce similar dynamics, creating strong strain in their vicinity, where the subgrid model acts to remove energy from the resolved scales, as evidenced by the isosurfaces of the subgrid energy flux.

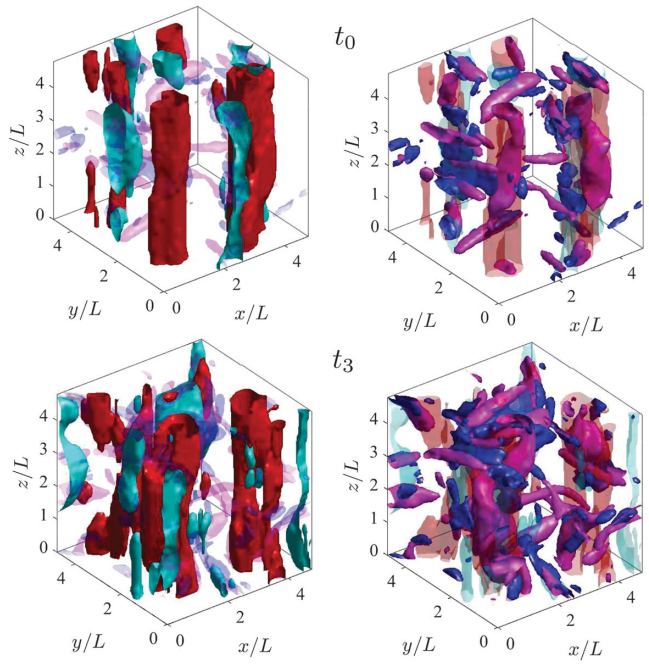

FIG. 3. Visualization of the spatial structure of the energy cascade at $t = t_0$ (top) and t_3 (bottom). Left: highlighting the isosurface of intense enstrophy of the filtered field $\bar{\boldsymbol{\omega}}^2 = 2.5\langle\bar{\boldsymbol{\omega}}^2\rangle_{st}$ (red) and energy transfer $s(\boldsymbol{x},t_3;l) = 3.0\langle s(l)\rangle_{st}$ (cyan) at $l = 1.6L$. Right: highlighting the isosurface of enstrophy $\boldsymbol{\omega}^2 = 2.5\langle\boldsymbol{\omega}^2\rangle_{st}$ (magenta) and subgrid energy flux $\epsilon = 3.0\langle\epsilon\rangle_{st}$ (blue). Animation available online [29].

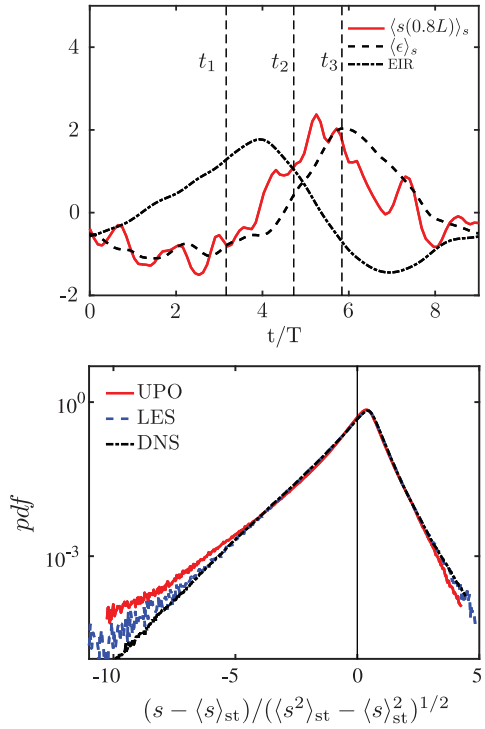

FIG. 4. Top: time evolution of the volume-averaged energy injection rate (EIR) $\langle \gamma \boldsymbol{f}\cdot\boldsymbol{u}\rangle_s$, the volume-averaged energy transfer $\langle s(0.8L)\rangle_s$, and the volume-averaged subgrid transfer $\langle\epsilon\rangle_s$, starting from $t_0=0$. Signals are normalized by subtracting the temporal mean and dividing by the standard deviation in time. Bottom: probability density function of local energy transfer events $s(\boldsymbol{x},t;0.8L)$ for the UPO, the LES flow, and the DNS flow at $\mathrm{Re}_\lambda=111$.

We find further evidence for the presence of at least one full step of the energy cascade in the analysis of the temporal signals of the energy injection rate, the interscale energy flux and the subgrid energy transfer, which are shown in Fig. 4 (top). The peak in the energy injection rate precedes the peak in subgrid energy transfer and between the two we observe a peak in energy transfer at an intermediate scale. This time delay reproduces the cyclic dynamics observed in HIT [13–15], evidencing the presence of an inertial gap between the energy-injection scales and the small scales. From t_0 to t_1, the large-scale vortex columns grow under the influence of the external force. Between t_1 and t_2 they break down, feeding the cascading process that leads to strong subgrid dissipation at t_3. The statistics of local energy fluxes in physical space also resemble that of fully developed turbulence. In Fig. 4 (bottom) we show the PDF of $s(\boldsymbol{x},t;0.8L)$, which shows wide tails and collapses well onto that of turbulent LES and the DNS described above. Energy backscatter, a characteristic feature of the energy cascade [30–32], also indicates the presence of healthy inertial-range dynamics. Intermittency, which is captured by the LES model, is manifest in the statistics of local energy transfer. In Table I we present the flatness factor of the local energy fluxes at different scales, $F_4(s)=\langle(s-\langle s\rangle_{st})^4\rangle_{st}/\langle s^2-\langle s\rangle^2_{st}\rangle^2_{st}$. Values are in the range reported by Cerutti and Meneveau [21] for fully developed turbulence and increase with decreasing scale.

TABLE I. Flatness factor of local energy transfer $s(\boldsymbol{x},t;l)$ at different scales. The flatness factor of the local subgrid fluxes $\epsilon=2\nu_T S_{ij}S_{ij}$ is $F_4(\epsilon)=22.9$.

l/L	1.6	1.2	0.8	0.4	0.2
$F_4(s)$	10.7	11.8	13.9	18.4	22.6

Conclusion.—We have presented a UPO in turbulent LES and have demonstrated that the periodic dynamics bear the hallmarks of the energy cascade process: a time delay between the maximum of energy input, the energy transfer at intermediate scales, and the dissipation; and spatial intermittency and $-5/3$ scaling in the energy spectrum. Direct visualization of the UPO reveals a complex spatiotemporal structure, where vortical dynamics overlap with energy transfer events in agreement with the scenario proposed by Goto *et al.* [15]. The results reported here required several months of computing on modern GPU cards, due to the poor conditioning of the linear problems associated with Newton's method and the slow convergence of Krylov subspace iteration. Likely owing to these computational bottlenecks, results on invariant solutions in LES have only recently started to appear. To the best of our knowledge, none concern time-periodic, scale-invariant dynamics. Sasaki *et al.* [33] computed UPOs in Couette flow, but did not attain a large enough separation of scales to observe the scaling laws typical of wall-bounded turbulence. Inertial range dynamics were likewise out of the scope of the prequel to the current work [22]. Sekimoto and Jiménez [34] studied a homogeneous shear layer with periodic boundary conditions. They computed several traveling wave solutions at significant scale separation, but these do not exhibit Kolmogorov scaling, possibly because their dynamics are too restricted.

We expect that significant improvements to the algorithms will be needed in order to compute a large number of UPOs in systems with a wide range of active length and timescales. The goal of this computation is to parse scale-invariant dynamics with periodic orbit theory (POT) [17]. In POT, UPOs are regarded as "templates" of chaotic dynamics and they are used in an algorithmic way to compute physically relevant mean quantities. POT has been successfully applied to spatially extended dynamics [35], but systems with a wide scale separation in more than one spatial dimension have so far proven elusive. We hope that the current work will serve as a proof of principle that templates of turbulence can be found, as well as the starting point of an investigation of cascade dynamics based on tracking vortical structures, Lyapunov vectors, and other quantities that can readily be computed for UPOs.

This research was partially funded by the COTURB program of the European Research Council (ERC-2014.AdG-669505). L. v. V. was supported by an NSERC Discovery Grant (No. 355849-2013). G, K. was supported by the Grant-in-Aid for Scientific Research program of the Japan Society for the Promotion of Science (No. 25249014 and No. 26630055). The authors gratefully acknowledge the computer resources at Minotauro and the technical support provided by Barcelona Supercomputing Center (FI-2017-3-0034).

*Corresponding author.
lennaert.vanveen@uoit.ca
†alberto@torroja.dmt.upm.es
‡kawahara@me.es.osaka-u.ac.jp

[1] M. L. Goldstein, D. A. Roberts, and W. H. Matthaeus, Annu. Rev. Astron. Astrophys. **33**, 283 (1995).
[2] N. Mordant and B. Miquel, Phys. Rev. E **96**, 042204 (2017).
[3] C. F. Barenghi, V. S. L'vov, and P.-E. Roche, Proc. Natl. Acad. Sci. U.S.A. **111**, 4683 (2014).
[4] A. N. Kolmogorov, Dokl. Akad. Nauk SSSR **30**, 301 (1941); Proc. R. Soc. A **434**, 9 (1991).
[5] A. N. Kolmogorov, J. Fluid Mech. **13**, 82 (1962).
[6] H. L. Grant, R. W. Stewart, and A. Moilliet, J. Fluid Mech. **12**, 241 (1962).
[7] J. C. Kaimal, J. C. Wyngaard, Y. Izumi, and O. R. Coté, Q. J. R. Meteorol. Soc. **98**, 563 (1972).
[8] T. Ishihara, K. Morishita, M. Yokokawa, A. Uno, and Y. Kaneda, Phys. Rev. Fluids **1**, 082403(R) (2016).
[9] L. F. Richardson, *Weather Prediction by Numerical Process* (Cambridge University Press, Cambridge, England, 1922).
[10] T. S. Lundgren, Phys. Fluids **25**, 2193 (1982).
[11] M. V. Melander and F. Hussain, Phys. Rev. E **48**, 2669 (1993).
[12] M. P. Brenner, S. Hormoz, and A. Pumir, Phys. Rev. Fluids **1**, 084503 (2016).
[13] J.-F. Pinton, P. C. W. Holdsworth, and R. Labbé, Phys. Rev. E **60**, R2452 (1999).
[14] J. I. Cardesa, A. Vela-Martín, S. Dong, and J. Jiménez, Phys. Fluids **27**, 111702 (2015).
[15] S. Goto, Y. Saito, and G. Kawahara, Phys. Rev. Fluids **2**, 064603 (2017).
[16] T. Yasuda, S. Goto, and G. Kawahara, Fluid Dyn. Res. **46**, 061413 (2014).
[17] P. Cvitanović, J. Fluid Mech. **726**, 1 (2013).
[18] J. Smagorinsky, Mon. Weather Rev. **91**, 99 (1963).
[19] M. Lesieur and O. Métais, Annu. Rev. Fluid Mech. **28**, 45 (1996).
[20] M. Linkmann, M. Buzzicotti, and L. Biferale, J. Turbul. **19**, 493 (2018).
[21] S. Cerutti and C. Meneveau, Phys. Fluids **10**, 928 (1998).
[22] L. van Veen, A. Vela-Martín, G. Kawahara, and T. Yasuda, Fluid Dyn. Res. **51**, 011411 (2019).
[23] D. Viswanath, J. Fluid Mech. **580**, 339 (2007).
[24] W. D. McComb, A. Berera, S. R. Yoffe, and M. F. Linkmann, Phys. Rev. E **91**, 043013 (2015).
[25] J. C. Vassilicos, Annu. Rev. Fluid Mech. **47**, 95 (2015).
[26] P. K. Yeung and J. G. Brasseur, Phys. Fluids **3**, 884 (1991).
[27] G. Bellani and E. A. Variano, Exp. Fluids **55**, 1646 (2014).
[28] J. Jiménez, Phys. Fluids A **4**, 652 (1992).
[29] See Supplemental Material at http://link.aps.org/supplemental/10.1103/PhysRevLett.123.134502 for animation of the UPO. In red: isosurface of the enstrophy filtered at $l = 1.6L$ at 2.5 times its spatio-temporal average. In cyan: isosurface of the unfiltered enstrophy at 2.5 times its spatio-temporal average. Note, that there is a shift of 0.85 times the grid spacing (of 1/64 times the box size) over one period.
[30] U. Piomelli, W. H. Cabot, P. Moin, and S. Lee, Phys. Fluids A **3**, 1766 (1991).
[31] V. Borue and S. A. Orszag, J. Fluid Mech. **366**, 1 (1998).
[32] G. L. Eyink and H. Aluie, Phys. Fluids **21**, 115107 (2009).
[33] E. Sasaki, G. Kawahara, A. Sekimoto, and J. Jiménez, J. Phys. Conf. Ser. **708**, 012003 (2016).
[34] A. Sekimoto and J. Jiménez, J. Fluid Mech. **827**, 225 (2017).
[35] X. Ding, H. Chaté, P. Cvitanović, E. Siminos, and K. A. Takeuchi, Phys. Rev. Lett. **117**, 024101 (2016).